Reactive Quenching of OH $A\ ^2\Sigma^+$ in Collisions with Molecular Deuterium via Nonadiabatic Passage through a Conical Intersection

Michael W. Todd,† David T. Anderson,‡ and Marsha I. Lester*

Department of Chemistry, University of Pennsylvania, Philadelphia, Pennsylvania 19104-6323

Received: July 11, 2001

The D and H atom products from collisional quenching of OH $A\ ^2\Sigma^+$ ($v = 0$) by D_2 have been examined through Doppler spectroscopy using two-photon ($2\ ^2S \leftarrow\leftarrow 1\ ^2S$) laser-induced fluorescence. A bimodal Doppler profile is observed for the D atoms, indicating that two different velocity distributions result from the OH $A\ ^2\Sigma^+ + D_2 \rightarrow D + HOD$ reaction. Nearly 40% of the products are H atoms produced in the OH $A\ ^2\Sigma^+ + D_2 \rightarrow H + D_2O$ reaction with a single Gaussian profile. The two components of the D atom kinetic energy distribution are characterized by translational temperatures of approximately 1200 and 10 000 K and on average account for 4% and 30% of the available energy. The H atom products accommodate about 37% of the available energy and are described by a 13 000 K temperature. The translational energy distributions of the H/D atom products are attributed to two dynamical pathways through the strong nonadiabatic coupling region at the HO−D_2 conical intersection. The narrow "cold" distribution of D atoms arises from an abstraction reaction in a direct passage through the conical intersection region. The broad statistical distribution observed for both D and H atom products suggests that the HO−D_2 collision pair lives long enough on the excited-state surface for energy to randomize before evolving through the conical intersection that leads to products.

Introduction

The complex chemistry that occurs in atmospheric and combustion environments is often monitored through the concentration, temperature, and lifetime of the OH radical intermediate.[1,2] The most common way to detect these OH radicals is by the laser-induced fluorescence (LIF) method on the $A\ ^2\Sigma^+ - X\ ^2\Pi$ electronic transition.[3] Collisions with partners prevalent under these conditions, however, are known to quench the OH $A\ ^2\Sigma^+$ fluorescence rather effectively.[4,5] For example, quenching of OH $A\ ^2\Sigma^+$ ($v = 0$) by simple collision partners such as N_2 and H_2/D_2 have cross sections of approximately 3 and 10 Å^2 at 300 K, while other partners such as CH_4 and H_2O have quenching cross sections that are an order of magnitude larger.[6−9] The sizable magnitude of these cross sections requires that quenching be taken into account when using the LIF method for quantitative determination of OH radical concentrations and population distributions.[10] As a result, the cross sections for quenching of OH $A\ ^2\Sigma^+$ by collision partners present in atmospheric and combustion environments have been systematically evaluated over the past 25 years.

Quenching collisions facilitate the efficient removal of OH population from the excited $A\ ^2\Sigma^+$ electronic state by introducing nonradiative decay pathways.[11,12] These pathways can lead to ground-state OH $X\ ^2\Pi$ radicals (nonreactive quenching) or reaction products. Only recently have experimental and theoretical studies started to examine the outcome of these electronic quenching events. This group has examined the reactive quenching of OH $A\ ^2\Sigma^+$ by molecular hydrogen through Doppler spectroscopy of the H atom products.[13] Wine and co-workers have investigated the production of N_2O from collisional quenching of OH $A\ ^2\Sigma^+$ by N_2,[14] and considered its importance in the atmospheric budget of N_2O. Finally, Schatz and co-workers have used a trajectory surface hopping method to explore the quenching of OH $A\ ^2\Sigma^+$ by transient H atoms,[15] a species thought to play a key role in flames. Their calculations indicate that three decay channels are significant: nonreactive quenching, atom exchange with quenching, and reaction yielding O (^{1}D) + H_2 products.

The quenching of OH $A\ ^2\Sigma^+$ by molecular hydrogen has also been the subject of numerous theoretical studies[12,16−18] and has emerged as a benchmark system for investigation of the nonadiabatic processes that lead to quenching. Recent ab initio calculations of the interaction energy for H_2 with OH in its ground $X\ ^2\Pi$ and excited $A\ ^2\Sigma^+$ electronic states identified specific orientations that lead to conical intersections between the ground- and excited-state adiabatic surfaces.[12,16−18] For the T-shaped HO−H_2 orientation illustrated in Figure 1, the ground- and excited-state surfaces are predicted to intersect ∼1.4 eV below the OH $A\ ^2\Sigma^+ + H_2$ asymptote. Two pathways exit from the conical intersection: a nonreactive quenching pathway follows down to OH $X\ ^2\Pi + H_2$, and a reactive pathway generates $H + H_2O$ after passing through the H_3O intermediate. For this C_{2v} configuration, there is little or no barrier separating the OH $A\ ^2\Sigma^+ + H_2$ reactants from the conical intersection region.[12,18] These ab initio calculations also suggest that the water product will be produced with a large degree of internal excitation due to the considerable structural changes that must occur between the conical intersection region and the $H + H_2O$ asymptote. Further theoretical work by Yarkony has identified several seams of conical intersections that may influence the quenching dynamics: a symmetry-allowed C_{2v} seam, a symmetry-allowed $C_{\infty v}$ seam, and a C_s seam that bridges the region

* To whom correspondence should be addressed. Fax: 215-573-2112. E-mail: milester@sas.upenn.edu.

† Present address: Informed Diagnostics, 1050 Duane Avenue, Suite I, Sunnyvale, CA 94086.

‡ Present address: Department of Chemistry, University of Wyoming, Laramie, WY 82071-3838.

10.1021/jp012674h CCC: $20.00
Published on Web 10/13/2001

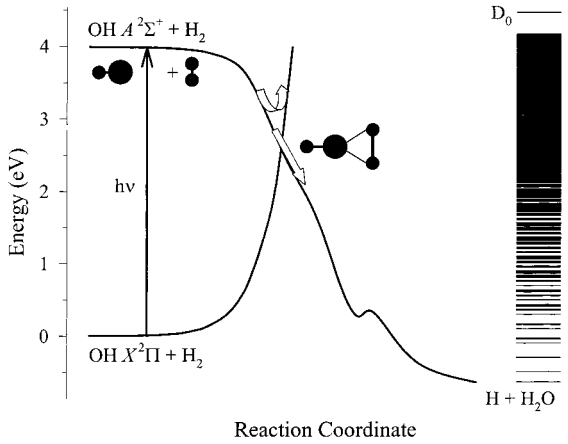

Figure 1. Simplified one-dimensional reaction coordinate for quenching of electronically excited OH $A\,^2\Sigma^+$ radicals by H_2 (adapted from ref 12), illustrating the conical intersection in the T-shaped HO−H_2 orientation. The diagram illustrates two distinct pathways that exit from the conical intersection leading to nonreactive quenching (OH $X\,^2\Pi + H_2$) or reactive quenching ($H + H_2O$) after passing through an H_3O local minimum. The stylized arrows depict direct and indirect passage through the conical intersection region. The H_2O product can be formed with a large degree of internal excitation as a result of the structural changes that occur between the conical intersection and the asymptote. The density of H_2O vibrational states and bond dissociation energy (D_0) are shown in the rightmost column.

between the two other seams.[17,18] However, a large barrier is likely to limit access to the $C_{\infty v}$ intersection in low-energy collisions of OH $A\,^2\Sigma^+$ with H_2.

Recently, we demonstrated that reactive quenching is a significant decay channel for electronically excited OH $A\,^2\Sigma^+$ ($v' = 0$) in collisions with molecular hydrogen.[13] We employed Doppler spectroscopy to characterize the H atom products from the OH $A\,^2\Sigma^+$ ($v' = 0$) + $H_2 \rightarrow H + H_2O$ quenching reaction. The observed H atom velocity distribution was bimodal and could be characterized by translational temperatures of approximately 1100 and 14 000 K. Conservation of energy dictates that H_2O is also produced with a bimodal internal energy distribution: a narrow "hot" internal energy distribution with an average energy of 4.6 eV and a broad statistical distribution with an average internal energy of 2.7 eV. We interpreted the bimodal distribution as arising from two different dynamical pathways through the conical intersection region. For instance, the reactants could pass through the conical intersection by the direct and indirect processes depicted through the stylized arrows in Figure 1. The collision partners could evolve directly through the conical intersection in a single pass or, alternatively, they could miss the conical intersection on the first approach, become momentarily trapped on the upper adiabatic surface, and eventually funnel through the conical intersection region.

This work extends our reactive quenching studies to OH $A\,^2\Sigma^+$ ($v' = 0$) + D_2 to provide additional mechanistic information on this fundamental nonadiabatic process. The isotopic substitution experiments reveal a surprising result: reactive quenching generates both D and H atom products. As shown in this paper, the H/D isotope and velocity distributions demonstrate that both abstraction- and insertion-like mechanisms are operative as the collision pair evolves through the conical intersection region(s).

Experiment

Reactive-quenching experiments have been carried out in the collisional region of a pulsed supersonic expansion, as described

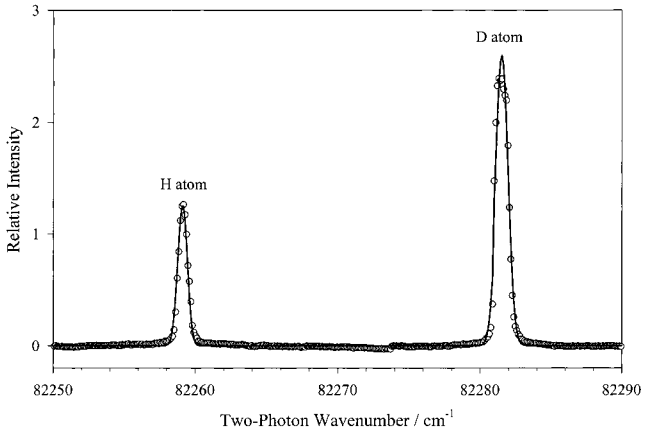

Figure 2. Background H/D atoms detected by the probe laser on the two-photon ($2\,^2S \leftarrow\leftarrow 1\,^2S$) atomic hydrogen and deuterium transitions in the absence of electronic excitation of OH. The background H/D atoms originate from photolysis of HNO_3 and/or reaction of ground-state OH $X\,^2\Pi$ radicals with D_2 in the carrier gas. This background signal is subtracted from that obtained with both pump and probe lasers to obtain the H/D signal attributed to reactive quenching.

previously.[13] In the present work, HNO_3 (90 wt %) is entrained in a 30% D_2 (UHP; 99.7% isotopic enrichment) balance He carrier gas at 150 psi backing pressure and pulsed into a vacuum apparatus. The OH radicals are formed by 193 nm photolysis (unpolarized) of HNO_3 at the exit of a quartz capillary tube (0.3 mm bore) that is attached to the faceplate of a pulsed valve. Pump and probe lasers intersect the pulsed supersonic expansion approximately 2 mm downstream from the exit of the capillary tube. The pump laser promotes OH radicals to the excited $A\,^2\Sigma^+$ electronic state with $v = 0$ and $J = {}^3/_2$ on the $Q_1(1)$ transition near 308 nm.[19] After a 20 ns delay, the time estimated for approximately one collision with a 10 $Å^2$ quenching cross section[6−8] at 150 K, the probe laser monitors the production of H/D atoms by two photon ($2\,^2S \leftarrow\leftarrow 1\,^2S$) laser-induced fluorescence at 243 nm.[20,21]

The pump beam at 308 nm is generated by frequency-doubling (KDP) the output of a Nd:YAG-pumped dye laser (30 mJ, 7 ns, 0.08 cm^{-1}). The probe beam at 243 nm (12−15 mJ, 4 ns, with an effective two-photon line width of 0.5 cm^{-1} fwhm) is produced by frequency-doubling (BBO) the output of an injected-seeded Nd:YAG-pumped optical parametric oscillator (Continuum Sunlite OPO). The pump and probe lasers are counterpropagated into the vacuum apparatus with parallel polarization, gently focused with 50 cm focal length lenses, and carefully spatially overlapped in the interaction region. The probe-laser-induced Lyman-α fluorescence is detected with a solar blind photomultiplier tube after passing through a notch filter. The resultant signal is then preamplified, integrated, and transferred to a laboratory computer.

The photolysis of nitric acid[22] and subsequent reaction of ground-state OH $X\,^2\Pi$ radicals with D_2 in the carrier gas[23,24] creates a "background" of H and D atoms in the supersonic expansion. Because these H and D atoms are created at the exit of the capillary tube where photolysis occurs, they can be cooled significantly by collisions[25] in the supersonic expansion before they reach the probe laser interaction region (∼2 mm). As shown in Figure 2, scans of the probe laser frequency reveal Doppler profiles for the background H and D atoms that are well-described by Gaussian distribution functions with breadths of 0.75 and 0.95 cm^{-1} (fwhm), respectively. Probing further downstream of the nozzle exit (∼15 mm) enables additional cooling of the background H and D atoms and yields line profiles that are limited by the probe laser bandwidth.

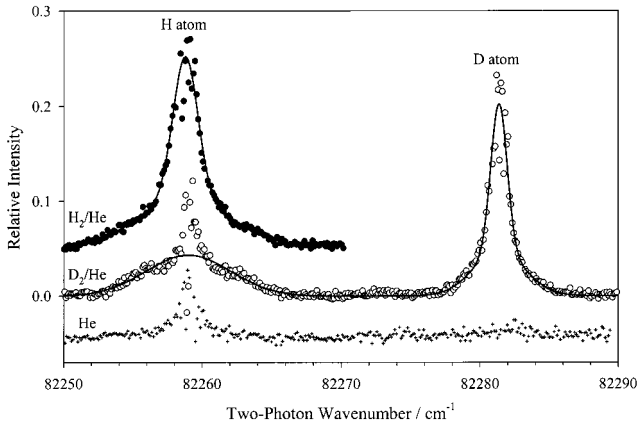

Figure 3. Isotopic substitution experiments reveal that reactive quenching of OH $A\ ^2\Sigma^+$ by D_2 yields D + HOD and H + D_2O products. The D and H atom signals (○) are the pump-laser-induced signals obtained in D_2/He carrier gas after subtracting the background signal (Figure 2). The H atom signal from reactive quenching of OH $A\ ^2\Sigma^+$ in a H_2/He carrier gas (●) is shown for comparison. Finally, a small pump-induced H atom signal is seen near line center in He (+), H_2/He, and D_2/He carrier gases that is attributed to reactive quenching of OH $A\ ^2\Sigma^+$ by a component in the HNO_3 sample.

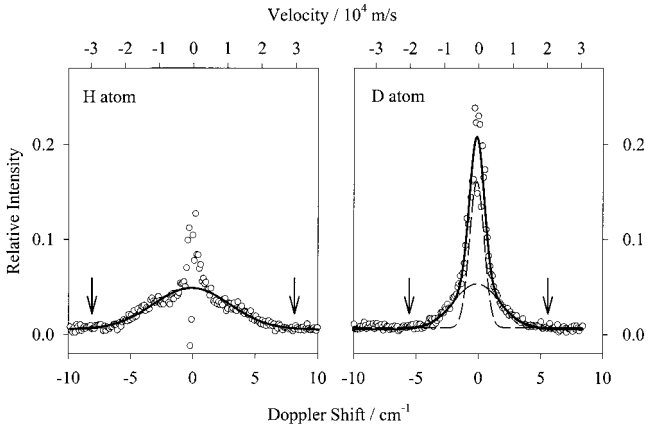

Figure 4. Doppler profiles observed for D and H atom products from reactive quenching of OH $A\ ^2\Sigma^+$ in collisions with D_2 and corresponding velocity distributions. The D atom profile is best represented by the sum of two Gaussian functions, indicating a bimodal velocity distribution characterized by translational temperatures of 1200 and 10 000 K. A single Gaussian is used to fit the H atom profile, illustrating the broad velocity distribution observed for the H atom products with a temperature of 13 000 K. The arrows indicate the calculated energetic limits for the Doppler shift.

To distinguish between the background H/D atoms and those produced by reactive quenching of electronically excited OH $A\ ^2\Sigma^+$ in collisions with D_2, a standard pump laser ON−OFF subtraction scheme is employed. This is implemented by operating the pump laser (5 Hz) at one-half the repetition rate of the probe laser (10 Hz). The H/D atom signal arising from the probe laser alone (OFF) is subtracted from that resulting from the combination of both pump and probe lasers (ON) on alternating laser pulses. Typically, 50 ON and 50 OFF data points are collected to yield the pump-laser-induced H/D atom signal attributed to reactive quenching. The pump-laser-induced H/D signals (ON) are much larger than the background signals (OFF) for most of the frequencies encompassing the Doppler profiles that result from reactive quenching, except at line center where the pump-laser-induced H/D signals are only ∼10% of the background signal level (see Figures 2 and 3). This gives rise to additional noise in the subtracted signal at line center. As a result, the central region of the Doppler profiles corresponding to the fwhm of the background H or D atoms was not included in the fits.

The pump laser was calibrated using the well-documented line positions for OH transitions in the $A\ ^2\Sigma^+ - X\ ^2\Pi$ 0−0 region.[19] The absolute frequency of the probe laser was determined from the well-known two-photon ($2\ ^2S \leftarrow\leftarrow 1\ ^2S$) atomic transitions of H and D atoms.[20] In addition, relative frequency markers were obtained by passing residual 486 nm radiation from the OPO through an Etalon (4.17 mm thick, 0.8202 cm^{-1} free spectral range). The improved frequency calibration procedures for the probe laser have resulted in slightly revised values for the Doppler shifts, H atom velocity distributions, and translational temperatures of the H atom products from OH $A\ ^2\Sigma^+ + H_2$ quenching (see Table 1) that supersede the previously reported values.[13]

Results and Analysis

The Doppler profiles resulting from collisional quenching of OH $A\ ^2\Sigma^+$ ($v = 0$, $J = {}^3/_2$) by D_2 are shown in Figure 3. Most of the reactive quenching signal is centered about the atomic deuterium two-photon ($2\ ^2S \leftarrow\leftarrow 1\ ^2S$) transition at 82 281.5 cm^{-1}, although a broad feature is also observed in the vicinity of the atomic hydrogen transition at 82 259.1 cm^{-1}. The D atoms result from D−D bond breakage as OH $A\ ^2\Sigma^+$ reacts with D_2 to form HOD. The H atoms can only arise from breaking the O−H bond in a reactive quenching process that produces D_2O. For comparison, the previously reported Doppler profile for H atoms resulting from reactive quenching of OH $A\ ^2\Sigma^+$ ($v = 0$, $J = {}^3/_2$) by H_2 is also displayed in Figure 3 (offset from zero for clarity).[13]

A series of experimental tests were performed to make sure that the pump-laser-induced signal arises from reactive quenching of OH $A\ ^2\Sigma^+$ by D_2. First, when the 193 nm photolysis laser was blocked, no subtracted signals were observed, because no OH radicals were produced. Second, experiments were carried out in a pure He carrier gas (see Figure 3), eliminating D_2 in the expansion. No pump-laser-induced D atom signal was found, although a small pump-induced H atom signal was observed with a narrow Doppler profile as reported previously.[13] This same narrow Doppler profile is seen near line center of the H atom transition in H_2/He and D_2/He carrier gases and is presumably due to reactive quenching of OH $A\ ^2\Sigma^+$ with a component of the HNO_3 sample. Third, no pump-induced signal was detected when the pump laser was detuned from the OH $Q_1(1)$ line. However, analogous pump-induced Doppler profiles were observed when the pump laser was tuned to OH $P_1(1)$ and $R_1(1)$ lines, thereby producing initial OH $A\ ^2\Sigma^+$ ($v = 0$) states with $J = {}^1/_2$ and ${}^5/_2$. Finally, the pump laser induced signal disappears if the pump−probe laser interaction region is moved downstream into the collision-free portion of the supersonic expansion. Thus, the pump-induced D and H atom signals in D_2/He carrier gas are ascribed to collisions of OH $A\ ^2\Sigma^+$ with D_2 that lead to reactive quenching events.

The experimental Doppler profiles of the D and H atom products are replotted in Figure 4 as a function of their spectral shift with respect to line center (ν_0) of the H or D atom two-photon transition. The Doppler shifts are directly related to the velocity of the H/D atom products along the laser propagation axis, which is shown on the top axis. The maximum velocity of the D atoms is readily determined from the total energy available to the products of reactive quenching:

$$E_{AVL} = E_{h\nu} - \Delta H_{rxn} + E_{col} \qquad (1)$$

TABLE 1. Parameters Derived from Doppler Profiles of the H and D Atom Products from Reactive Quenching of OH $A\ ^2\Sigma^+$ by H_2 and D_2[a]

fwhm[b] (cm^{-1})	T (K)	$\langle E_{T,H}\rangle$ or $\langle E_{T,D}\rangle$ (eV)	$\langle E_T\rangle$ (eV)	$\langle f_T\rangle$
OH $A\ ^2\Sigma^+ + H_2 \rightarrow$ **H** $+ H_2O$ ($E_{AVL} = 4.72$ eV)[c,d]				
1.9(4)[e]	$1.1(5) \times 10^3$	0.14(6)	0.15(6)	0.03(1)
7.0(6)	$1.4(3) \times 10^4$	1.9(3)	2.0(4)	0.42(8)
OH $A\ ^2\Sigma^+ + D_2 \rightarrow$ **D** $+$ HOD ($E_{AVL} = 4.72$ eV)[d]				
1.4(3)[e]	$1.2(4) \times 10^3$	0.15(6)	0.17(6)	0.04(1)
4.1(5)	$1.0(2) \times 10^4$	1.3(3)	1.4(3)	0.30(6)
OH $A\ ^2\Sigma^+ + D_2 \rightarrow$ **H** $+ D_2O$ ($E_{AVL} = 4.80$ eV)[d]				
6.8(7)[e]	$1.3(3) \times 10^4$	1.7(3)	1.8(4)	0.37(8)

[a] Parameters included in the table are the breadth (fwhm), the translational temperature (T), the average H or D atom translational energy ($\langle E_{T,H}\rangle$ or $\langle E_{T,D}\rangle$), the average energy released into product translational energy ($\langle E_T\rangle$), and the fraction of available energy (E_{AVL}) deposited in translation of the products ($\langle f_T\rangle$). [b] The effective two-photon probe laser bandwidth (0.5 cm^{-1}) is much smaller than the fitted Doppler widths. [c] The parameters for the H atom products of OH $A\ ^2\Sigma^+$ reactive-quenching collisions with H_2 supersede an earlier report (ref 13) because of an improved frequency calibration procedure. [d] E_{AVL} takes into account changes in zero-point energies for the different isotopes of H_2O and H_2. [e] The uncertainties represent one standard deviation for a complete set of 16 (D_2/He) or 15 (H_2/He) measurements not the quality of an individual fit.

where $E_{h\nu} = 4.025$ eV for OH $A-X$ 0−0 electronic excitation,[19] $\Delta H_{rxn} = -0.645$ eV for the ground-state OH $X\ ^2\Pi + D_2 \rightarrow$ D + HOD reaction,[26] and a collision energy of $E_{col} \approx 0.05$ eV yields $E_{AVL} = 4.72$ eV. On the basis of conservation of linear momentum and energy, the maximum velocity of the D atom products is obtained using

$$v_D^{max} = \sqrt{\frac{2E_{AVL}}{m_D(1 + m_D/m_{HOD})}} \qquad (2)$$

An analogous expression is used to determine v_H^{max} for the H atom products from the OH $A\ ^2\Sigma^+ + D_2 \rightarrow H + D_2O$ reactive quenching process with $E_{AVL} = 4.80$ eV (taking into account the change in zero-point energy for different isotopes of water). This yields $v_D^{max} = 20\,200$ and $v_H^{max} = 29\,600$ m/s, corresponding to maximum Doppler shifts of ± 5.55 and ± 8.12 cm^{-1}, respectively. The experimental D and H atom Doppler profiles extend out to the calculated energetic limits, which are indicated by arrows in Figure 4.

The observed Doppler profiles are one-dimensional projections of three-dimensional velocity distributions along the laser propagation axis. The Doppler profiles are well-modeled with Gaussian distribution functions, indicating that the velocity distributions are spatially isotropic.[27,28] As shown in Figure 4, the D atom Doppler profile is best represented by the sum of two Gaussian functions, while the H atom profile is best fit to a single Gaussian function. The breadth (fwhm) of each Gaussian component is listed in Table 1.

The bimodal D atom Doppler profile indicates that two different velocity distributions result from reactive quenching of OH $A\ ^2\Sigma^+$ with D_2, while the H atoms are produced with a single velocity distribution. A translational temperature[27] can be derived for each Gaussian component by using the fitted breadth (fwhm) and assuming Boltzmann translational energy distributions for the D (or H) atom products:

$$T = \frac{\left(\frac{\text{fwhm}}{2\nu_0}\right)^2 m_D c^2}{2k \ln 2} \qquad (3)$$

The integrated area of each Gaussian component is directly proportional to the D or H atom number density with a given velocity distribution because the absorption coefficient of D atoms is precisely the same as that of H atoms.[29] This indicates that approximately 30% of the products are D atoms with an average translational temperature of 10 000 K, 30% are the balance of D atoms with a temperature of 1200 K, and the remaining 40% are H atoms with a temperature of 13 000 K. The average translational energy of the D atoms, $\langle E_{T,D}\rangle = 3kT/2$, is then converted from the lab frame to a center-of-mass frame to calculate the translational energy released to the D + HOD products, $\langle E_T\rangle = m_{HOD_2}/(m_{HOD}\langle E_{T,D}\rangle)$. An analogous procedure is used to convert $\langle E_{T,H}\rangle$ into $\langle E_T\rangle$ for the H + D_2O products. Finally, the fraction of the total energy imparted to the products as translational energy, $\langle f_T\rangle$, is calculated to be 0.04 and 0.30 for narrow and broad Doppler components of the D atom distribution, and $\langle f_T\rangle = 0.37$ for the H atom Doppler profile. Thus, we see that only a small fraction of the available energy is released to products as translational energy. These results are summarized in Table 1.

The translational temperatures of the D and H atom products are also converted into product translational energy distributions, $P(E_T)$, assuming a Maxwell−Boltzmann speed distribution:

$$P(E_T)\,dE_T = \frac{2}{\pi^{1/2}(kT)^{3/2}} E_T^{1/2}\, e^{-E_T/(kT)}\, dE_T \qquad (4)$$

The translational energy distributions for the D and H atoms resulting from reactive quenching of OH $A\ ^2\Sigma^+$ in collisions with D_2 are plotted in Figure 5. The $P(E_T)$ distributions obtained for quenching of OH $A\ ^2\Sigma^+$ by H_2 are also shown for comparison.[13] The integrated area of each $P(E_T)$ distribution is proportional to the number of D or H atom products with a given velocity distribution. In addition, the total probability for producing H/D atoms from reactive quenching of OH $A\ ^2\Sigma^+$ by D_2 (or H_2) has been normalized to 1. The broad $P(E_T)$ distributions have also been cut off at E_{AVL}, as required, even though the assumed functional form of the translational energy distribution would normally have a small tail extending to still higher energies.

After the translational energy release to products has been accounted for, the balance of available energy must be accommodated as internal excitation of the HOD or D_2O products. The HOD product is produced with a bimodal internal energy distribution: an extremely narrow component of "hot" HOD molecules with average energy of 4.6 eV and a broader component with an average internal energy of 3.3 eV. The D_2O product also has a broad internal energy distribution with an average energy of 3.0 eV. While the HOD and D_2O products are produced with a very large amount of internal excitation, it is not sufficient to cause dissociation of the water molecules.[30] Future experiments are planned to examine the quantum state distribution of these "hot" water molecules directly.

Discussion

The translational energy distributions of the H/D products and the H/D product branching ratio provide insights into the mechanism for reactive quenching of electronically excited OH $A\ ^2\Sigma^+$ radicals by D_2. In particular, they contain information about the evolution of the HO−D_2 collision pair through the conical intersection region. The experimental observables can reflect the restricted geometrical configuration in the vicinity of the conical intersection(s). In addition, they can reveal the dynamical pathways of the reactants as they pass through the

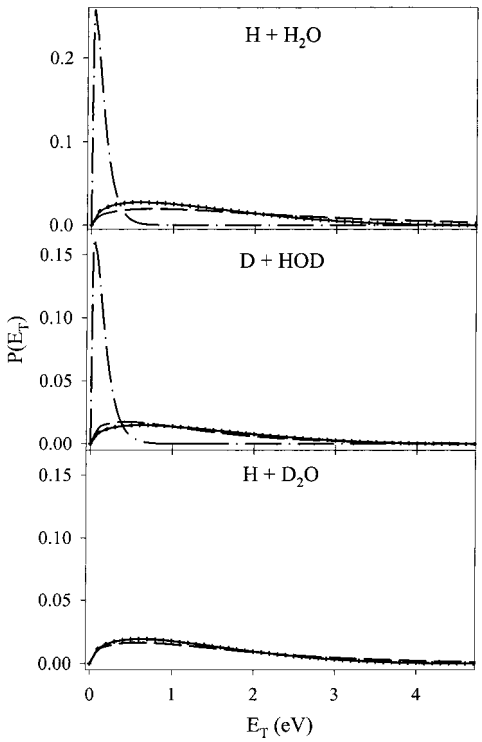

Figure 5. Translation energy distributions, $P(E_T)$, derived for the H and D atom products of reactive quenching of OH $A\ ^2\Sigma^+$ in collisions with H_2 and D_2. The integrated area of each $P(E_T)$ distribution reflects the fraction of H/D products with a given velocity distribution. Statistical distributions (solid line with crosshairs), based on the density of vibrational states for the recoiling products, compare favorably with the broad experimental distributions (dashed lines). The narrow translational energy distributions observed for $H + H_2O$ and $D + HOD$ products (dot−dash lines) are clearly nonstatistical. The corresponding internal energy distribution of the H_2O, HOD, or D_2O products can be readily obtained by subtracting the $P(E_T)$ distribution from the available energy (E_{AVL}).

nonadiabatic coupling region(s). These possibilities are considered in more detail in the discussion that follows.

The translational energy release to the D atom products from reactive quenching of OH $A\ ^2\Sigma^+$ by D_2 is analogous to that observed previously for the H atom products from OH $A\ ^2\Sigma^+$ collisions with H_2.[13] While the Doppler profiles are narrower for the D atom products as compared to those seen for the H atom products because of the increased mass of the D atom, their kinetic energy distributions turn out to be remarkably similar. Both the D and H atom products exhibit bimodal translational energy distributions with similar characteristics (Table 1).

The observation of H atom products from the reactive quenching of OH $A\ ^2\Sigma^+$ by D_2 was completely unexpected. Nevertheless, it is now shown to be a significant reaction channel with nearly 40% of the reactive quenching events following the OH $A\ ^2\Sigma^+ + D_2 \rightarrow H + D_2O$ pathway. The translational energy distribution for this channel (Table 1) is similar to the broad components observed for the H atom products from OH $A\ ^2\Sigma^+ + H_2$ as well as for the D atom products from OH $A\ ^2\Sigma^+ + D_2$.

The broad components of the translational energy distributions for the H/D atom products as well as the appearance of both D and H atom products suggest that the available energy is statistically distributed among the various product states. A statistical distribution would be expected if the HO−D_2 collision pair lived for a long period of time on the upper adiabatic surface, possibly making multiple traversals of the conical intersection region(s),[31] before undergoing the nonadiabatic event that produces D + HOD or H + D_2O products. To test this hypothesis, the experimental translational energy distributions (Figure 5) are compared with distributions predicted using a statistical model.[32] The statistical model assumes (a) complete vibrational energy randomization in the HO−D_2 (or HO−H_2) reactant pair and (b) that the probability of forming product pairs with a particular translational energy, $P(E_T)$, is proportional to the total density of product states. For simplicity, the total density of product states is modeled as the product of the density of vibrational states, $N(E_V)$, for the H_2O, HOD, or D_2O product and a term $E_T^{1/2}$ representing the three-dimensional translational density of states for the recoiling products, $P(E_T) = N(E_V)\ E_T^{1/2}$, where $E_T + E_V = E_{AVL}$. Rotational degrees of freedom are ignored in these calculations. The density of states was evaluated from a direct count of water vibrational states including anharmonicity corrections.[33] The resultant statistical translational energy distributions are plotted in Figure 5. The statistical distributions differ slightly from one another because of the different state densities for the three isotopes of water at a given E_V.

The statistical $P(E_T)$ distributions computed for the $H + H_2O$, $D + HOD$, and $H + D_2O$ products are generally in good accord with the broad $P(E_T)$ distributions observed experimentally for each of these product channels. To facilitate this comparison, the integrated areas of the statistical distributions were set equal to those of the broad components of the experimental distributions in Figure 5. The agreement with the broad $P(E_T)$ experimental distributions indicates that energy has randomized within the HO−D_2 (or HO−H_2) collision pair prior to passing through the conical intersection region(s). If H and D atom sites were equivalent in the statistical breakup of HO−D_2 (e.g., for a D_{3h} configuration at the conical intersection), then we would expect to observe an H:D ratio of 1:2, rather than the 4:3 ratio seen experimentally. The observed tendency to favor H atom products suggests a C_{2v} configuration at the conical intersection with an extended H−O bond and a close approach of O to D_2 as it inserts into the D−D bond (see Figure 7 of ref 16).

By contrast, the remaining D (or H) atom products exhibit a narrow translational energy distribution that is highly nonstatistical. The narrow "cold" $P(E_T)$ distribution arises from a nonadiabatic transition as the collision partners evolve directly through the conical intersection, most likely in a single pass. The D (or H) atom abstraction must occur rapidly to minimize energy redistribution within the HO−D_2 (or HO−H_2) system. This direct reaction leaves the HOD (or H_2O) products with very high average internal energies, $\langle E_{INT} \rangle = 4.6$ eV, in an extremely narrow distribution with a breadth of less than 0.2 eV. These water molecules are likely to have highly inverted vibrational population distribution, as found recently by Saykally and co-workers in the dissociative recombination of H_3O^+ ions with electrons, $H_3O^+ + e^- \rightarrow H_2O + H$, which may pass through the same H_3O conical intersection region(s) considered here on their way to forming water products.[34]

This high degree of internal excitation in the HOD (or H_2O) products from the direct reaction can be understood by comparing the geometries computed for the conical intersection region(s) with the equilibrium structure of the water product. For this comparison, we use representative configurations computed along the C_{2v}, $C_{\infty v}$, and C_s seams of the conical intersection by Hoffman and Yarkony.[18] After passing through the C_{2v} conical intersection, the newly formed HOD products will have an extended O−D bond length (1.5 Å) and large HOD bond angle (165°) compared with the equilibrium HOD structure (0.96 Å

and 105°). Starting from the $C_{\infty v}$ conical intersection, the newly formed HOD will have an extremely large HOD bond angle (180°) and an extended O−D bond length (1.2 Å). However, a substantial barrier[18] makes it unlikely that the $C_{\infty v}$ intersection will be accessible in low-energy collisions of OH $A\ ^2\Sigma^+$ with D_2 (or H_2). The C_s seam of conical intersection has configurations intermediate to those described above. In each case, the distorted structure of water formed at the conical intersection leads to highly vibrationally excited water products.

Conclusion

This work extends our investigation of reactive quenching of electronically excited OH $A\ ^2\Sigma^+$ ($v = 0$) radicals by molecular hydrogen through isotopic substitution and Doppler spectroscopy of the H/D atom products. We find that reactive quenching is a significant decay channel for low-energy collisions of OH $A\ ^2\Sigma^+$ with D_2, producing both D + HOD products and an unexpected H + D_2O channel. Analysis of the H/D Doppler profiles reveals a bimodal translational energy distribution for the D atom products, consisting of a broad statistical component and a narrow "cold" component that is highly nonstatistical. The H atom products are produced exclusively with a broad distribution. The kinetic energy distributions of the H/D atom products are attributed to two different dynamical pathways through the conical intersection region(s). A direct reaction can occur in which OH abstracts a D atom as the HO−D_2 collision partners pass rapidly through the conical intersection region. In addition, this nonadiabatic reaction can proceed by insertion of the O side of OH into the D_2 bond, most likely in a C_{2v} configuration, followed by unimolecular decomposition of the highly excited HO−D_2 species that produces both D and H atom products. The statistical translational energy release for these D and H atom products suggests that the HO−D_2 collision pair is sufficiently long-lived on the upper adiabatic surface for energy randomization to occur before the system evolves through the conical intersection region.

There are several questions concerning the collisional quenching of OH $A\ ^2\Sigma^+$ by H_2 that remain to be answered, and these will be the subject of future studies in this laboratory. Specifically, we want to determine the branching between nonreactive quenching (OH $X\ ^2\Pi$ + H_2) and reactive quenching (H + H_2O) pathways. In addition, we plan to examine the internal state distribution of the OH $X\ ^2\Pi$ products. And finally, we intend to evaluate the quantum-state distribution of the highly excited H_2O products. We hope that this experimental work will be complemented by theoretical studies of the dynamics associated with this fundamental nonadiabatic process.

Acknowledgment. This work has been supported by the Office of Basic Energy Sciences of the Department of Energy. Some financial support for this project has been obtained from the Air Force Office of Scientific Research. Partial equipment support has been provided by the Chemistry Division of the National Science Foundation. The authors thank Bethany V. Pond for valuable contributions to this project.

References and Notes

(1) Wayne, R. P. *Chemistry of Atmospheres*, 3rd ed.; Oxford University Press: Oxford, 2000.
(2) Glassman, I. *Combustion*, 3rd ed.; Academic Press: San Diego, CA 1996.
(3) Rothe, E. W.; Andresen, P. *Appl. Opt.* **1997**, *36*, 3971−4033.
(4) Lee, M. P.; Kienle, R.; Kohse-Hoeinghaus, K. *Appl. Phys. B: Lasers Opt.* **1994**, *B58*, 447−457.
(5) Crosley, D. R. *Adv. Ser. Phys. Chem.* **1995**, *3*, 256−317.
(6) German, K. R. *J. Chem. Phys.* **1976**, *64*, 4065−4068.
(7) McDermid, I. S.; Laudenslager, J. B. *J. Chem. Phys.* **1982**, *76*, 1824−1831.
(8) Copeland, R. A.; Dyer, M. J.; Crosley, D. R. *J. Chem. Phys.* **1985**, *82*, 4022−4032.
(9) Bailey, A. E.; Heard, D. E.; Henderson, D. A.; Paul, P. H. *Chem. Phys. Lett.* **1999**, *302*, 132−138.
(10) Kienle, R.; Lee, M. P.; Kohse-Hoeinghaus, K. *Appl. Phys. B: Lasers Opt.* **1996**, *B62*, 583−599.
(11) Crosley, D. R. *J. Phys. Chem.* **1989**, *93*, 6273−6282.
(12) Lester, M. I.; Loomis, R. A.; Schwartz, R. L.; Walch, S. P. *J. Phys. Chem. A* **1997**, *101*, 9195−9206.
(13) Anderson, D. T.; Todd, M. W.; Lester, M. I. *J. Chem. Phys.* **1999**, *110*, 11117−11120.
(14) Estupinan, E. G.; Stickel, R. E.; Wine, P. H. *Chem. Phys. Lett.* **2001**, *336*, 109−117.
(15) Schatz, G. C.; Fisher, B.; Grande, W.; Kumayama, K.; Pederson, L. A. *J. Phys. Chem. A* **2001**, *105*, 2515−2521.
(16) Yarkony, D. R. *J. Phys. Chem.* **1996**, *100*, 18612−18628.
(17) Yarkony, D. R. *J. Chem. Phys.* **1999**, *111*, 6661−6664.
(18) Hoffman, B. C.; Yarkony, D. R. *J. Chem. Phys.* **2000**, *113*, 10091−10099.
(19) Dieke, G. H.; Crosswhite, H. M. *J. Quant. Spectrosc. Radiat. Transfer* **1962**, *2*, 97−198.
(20) Hansch, T. W.; Lee, S. A.; Wallenstein, R.; Wieman, C. *Phys. Rev. Lett.* **1975**, *34*, 307−309.
(21) Cesar, C. L.; Fried, D. G.; Killian, T. C.; Polcyn, A. D.; Sandberg, J. C.; Yu, I. A.; Greytak, T. J.; Kleppner, D.; Doyle, J. M. *Phys. Rev. Lett.* **1996**, *77*, 255.
(22) Turnipseed, A. A.; Vaghjiani, G. L.; Thompson, J. E.; Ravishankara, A. R. *J. Chem. Phys.* **1992**, *96*, 5887−5895.
(23) Alagia, M.; Balucani, N.; Casavecchia, P.; Stranges, D.; Volpi, G. G. *J. Chem. Phys.* **1993**, *98*, 2459−2462.
(24) Strazisar, B. R.; Lin, C.; Davis, H. F. *Science* **2000**, *290*, 958−961.
(25) Park, J.; Shafer, N.; Bersohn, R. *J. Chem. Phys.* **1989**, *91*, 7861.
(26) Chase, M. W., Jr.; Curnutt, J. L.; Downey, J. R., Jr.; McDonald, R. A.; Syverud, A. N.; Valenzuela, E. A. *J. Phys. Chem. Ref. Data* **1982**, *11*, 695−940.
(27) Zare, R. N.; Herschbach, D. R. *Proc. IEEE* **1963**, *51*, 171−182.
(28) Tonokura, K.; Matsumi, Y.; Kawasaki, M.; Kasatani, K. *J. Chem. Phys.* **1991**, *95*, 5065−5071.
(29) Johnston, G. W.; Kornweitz, H.; Schechter, I.; Persky, A.; Katz, B.; Bersohn, R.; Levine, R. D. *J. Chem. Phys.* **1991**, *94*, 2749−2757.
(30) Ruscic, B.; Feller, D.; Dixon, D. A.; Peterson, K. A.; Harding, L. B.; Asher, R. L.; Wagner, A. F. *J. Phys. Chem. A* **2001**, *105*, 1−4.
(31) Martinez, T. J.; Ben-Nun, M.; Levine, R. D. *J. Phys. Chem. A* **1997**, *101*, 6389−6402.
(32) Ashfold, M. N. R.; Dixon, R. N.; Kono, M.; Mordaunt, D. H.; Reed, C. L. *Philos. Trans. R. Soc. London, Ser. A* **1997**, *355*, 1659−1676.
(33) Benedict, W. S.; Gailar, N.; Plyler, E. K. *J. Chem. Phys.* **1956**, *24*, 1139−1165.
(34) Michael, E. A.; Keoshian, C. J.; Wagner, D. R.; Anderson, S. K.; Saykally, R. J. *Chem. Phys. Lett.* **2001**, *338*, 277−284.